Supporting Information

Depositing CdS Nanoclusters on Carbon-modified $NaYF_4$:Yb,Tm Upconversion Nanocrystals for NIR-light Enhanced Photocatalysis

Meijie Tou,† Yuanyuan Mei,† Song Bai,* Zhengguo Luo, Yong Zhang and Zhengquan Li*

Institute of Physical Chemistry and Department of Chemistry, Zhejiang Normal University, Xinhua, Zhejiang 321004, P. R. China

E-mail: songbai@zjnu.edu.cn (S. Bai); zqli@zjnu.edu.cn (Z. Li)

† Equal contribution.

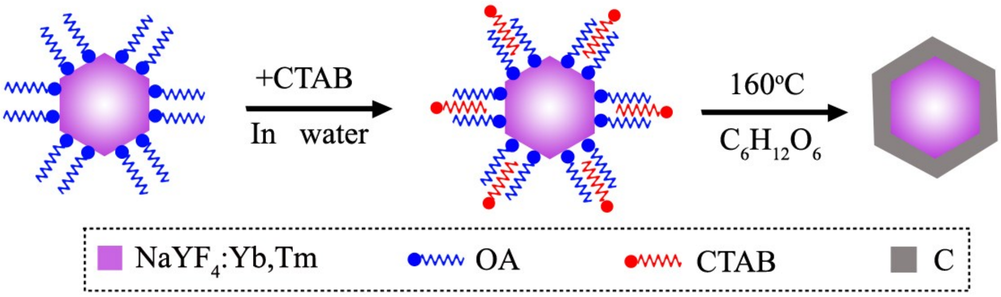

Figure S1. Schematic illustration of the reverse micelle method for the preparation of $NaYF_4$:Yb,Tm@C NPs. The surfactant CTAB serves as a surface-modifier on the oleic acid-capped $NaYF_4$:Yb,Tm NCs through van der Waals interaction, making the NCs water dispersible for hydrothermal coating of a carbon layer.

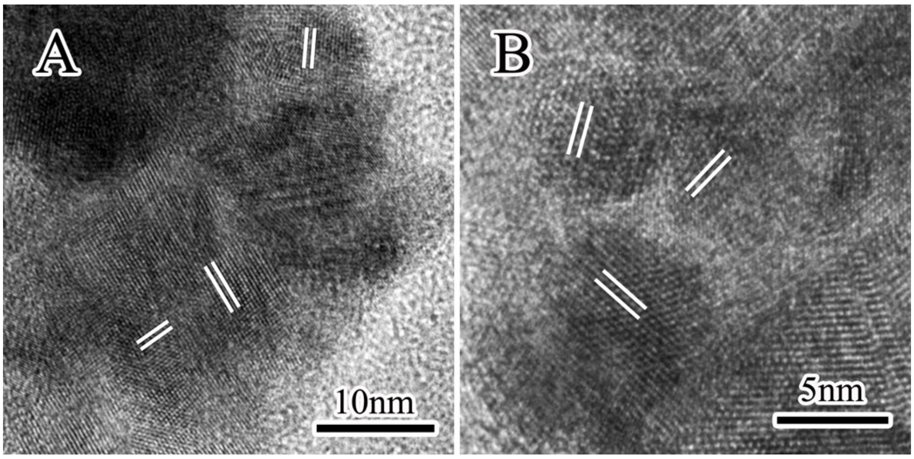

Figure S2. (A) and (B) are high-resolution TEM images of two different CdS nanoclusters on a single $NaYF_4$:Yb,Tm@C@CdS NP. Each tiny CdS NC exhibits clear lattice fringes, showing good crystallinities after microwave irradiation.

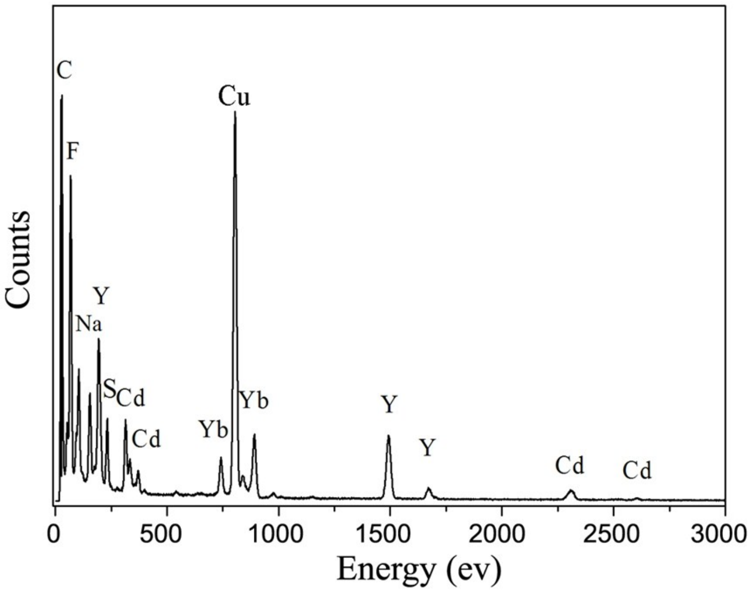

Figure S3. EDS analysis of the prepared $NaYF_4$:Yb,Tm@C@CdS NPs. The signal of Cu element is from the copper grid.

Atomic % by EDS							
Element	C	F	Na	Y	Yb	Cd	S
Proportion/%	57.1	23.0	2.7	3.1	1.5	0.9	1.2

Table S1. The content of different elements in the $NaYF_4$:Yb,Tm@C@CdS NPs detected by the EDS analysis. The high content of C element is from both the NPs and carbon film on the copper grid.

Atomic % by XPS							
Element	C	F	Na	Y	Yb	Cd	S
Proportion/%	29.8	39.2	7.53	7.89	3.86	3.36	4.08

Table S2. The content of different elements in the $NaYF_4$:Yb,Tm@C@CdS NPs detected by the XPS analysis.

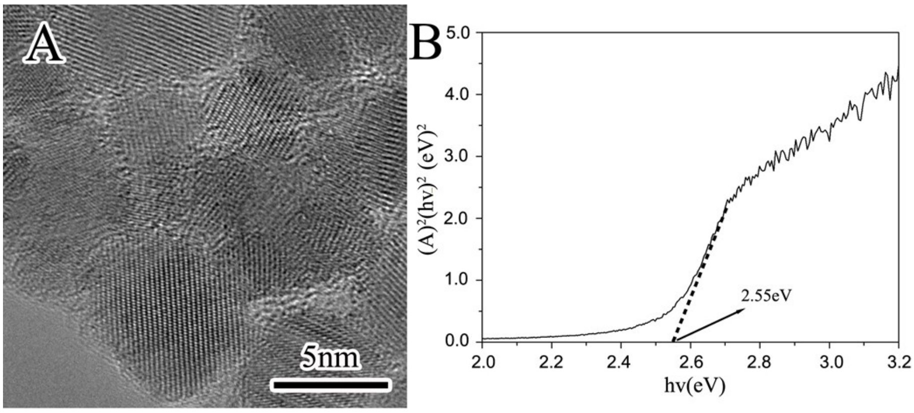

Figure S4. (A) TEM image of pure CdS NCs prepared by microwave irradiation without the addition of $NaYF_4$:Yb,Tm@C seeds; (B) Bandgap of the prepared CdS NCs calculated from their UV-Vis spectrum.

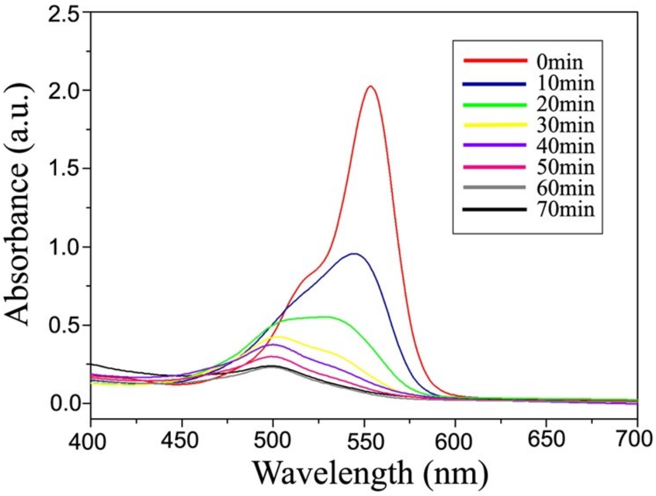

Figure S5. UV-Vis absorption spectra of the RhB solution catalyzed by the NaYF$_4$:Yb,Tm@C@CdS NPs under Vis-NIR irradiation band (400-2500 nm). The decrease in RhB concentration is obvious faster than that under Vis band (400-700 nm, see Fig. 7A).

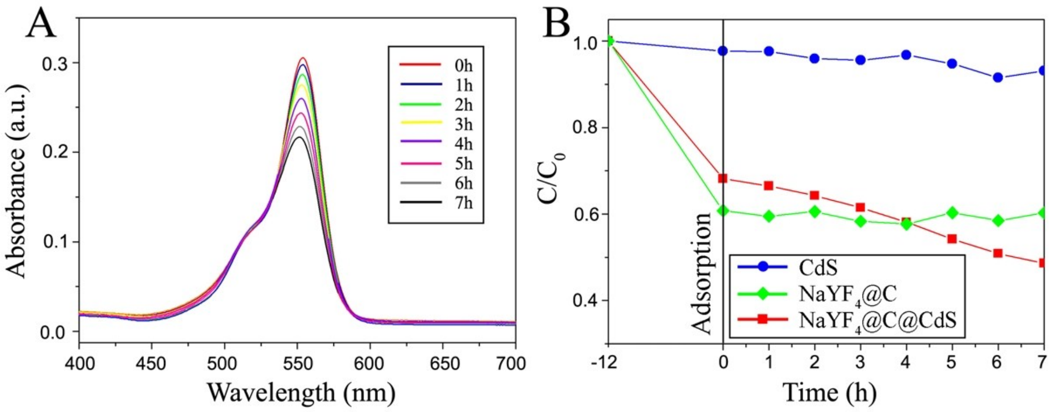

Figure S6. (A) UV-Vis absorption spectra of RhB solution catalyzed by the NaYF$_4$:Yb,Tm@C@CdS NPs under the 980-nm NIR laser; (B) Comparison of photocatalytic activities of different samples under the NIR laser. Note that the NaYF$_4$:Yb,Tm@C NPs show strong adsorption to dye molecules but does not show obvious catalytic activity.

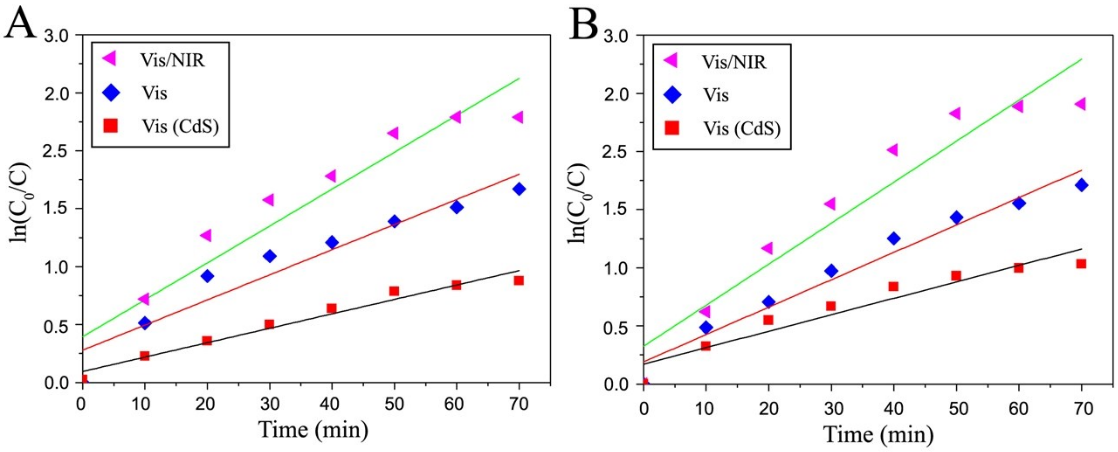

Figure S7. Apparent rate constants of the NaYF$_4$:Yb,Tm@C@CdS NPs on the degradation of RhB and MB solutions under different irradiation bands: (A) RhB solution; (B) MB solution.

Sample	**Fitted equation**	***k* (min^{-1})**	**Correlation coefficient R^2**
CdS(Vis)	y=0.01244x + 0.0948	0.01244	0.96338
NaYF$_4$@C@CdS(Vis)	y=0.02196x + 0.27866	0.02196	0.90680
NaYF$_4$@C@CdS(Vis/NIR)	y=0.03185x + 0.39490	0.03185	0.90669

Table S3. Apparent rate constant *k* for the RhB degradation over different samples and/or irradiation bands.

Sample	**Fitted equation**	***k* (min^{-1})**	**Correlation coefficient R^2**
CdS(Vis)	y=0.01415x + 0.17109	0.01415	0.90657
NaYF$_4$@C@CdS(Vis)	y=0.02355x + 0.19026	0.02196	0.95904
NaYF$_4$@C@CdS(Vis/NIR)	y=0.03528x + 0.39490	0.03248	0.90949

Table S4. Apparent rate constant *k* for the MB degradation over different samples and/or irradiation bands.

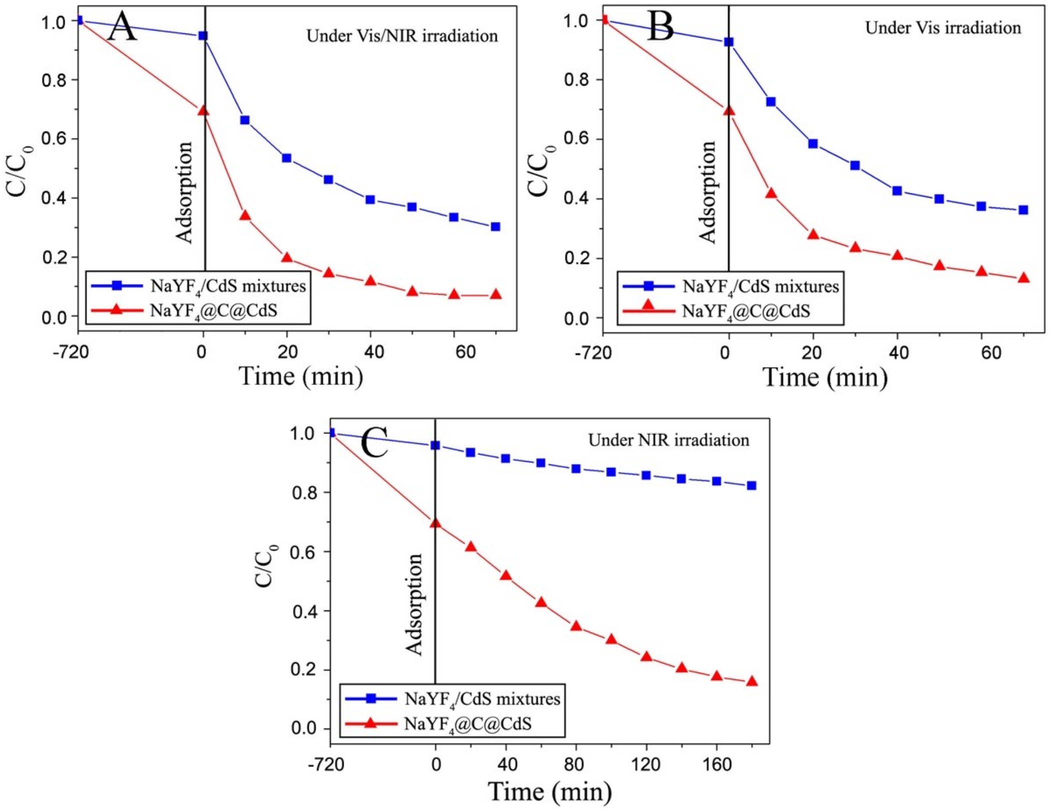

Figure S8. Comparison of photocatalytic activities between the mixture of $NaYF_4$:Yb,Tm/CdS and $NaYF_4$:Yb,Tm@C@CdS NPs under different irradiation bands: (A) Vis-NIR band; (B) Vis band; (C) NIR band. The amounts of $NaYF_4$:Yb,Tm and CdS in the mixture are the same as those in the $NaYF_4$:Yb,Tm@C@CdS NPs. The photocatalytic activity of this mixture is obviously lower than that of the $NaYF_4$:Yb,Tm@C@CdS NPs under different irradiation bands, particularly under the NIR band. This result indicates that the synthesis of uniform core-shell nanostructures with a carbon layer is crucial to their good photocatalytic properties.

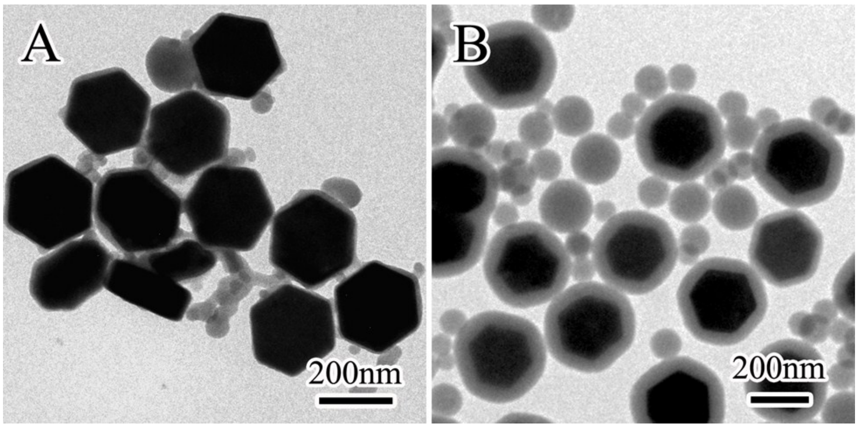

Figure S9. (A) and (B) are TEM images of samples prepared with different concentration of glucose: (A) 10 mg/mL; (B) 70 mg/mL. The synthesis of carbon shell with obvious different shell thickness, in contrast to the core NCs (200 nm), requires much diluted or concentrated glucose. In both cases, the uniformity of samples is not as good as that of the 30 nm-carbon-shell sample prepared with 40 mg/mL glucose (see Figure 2).

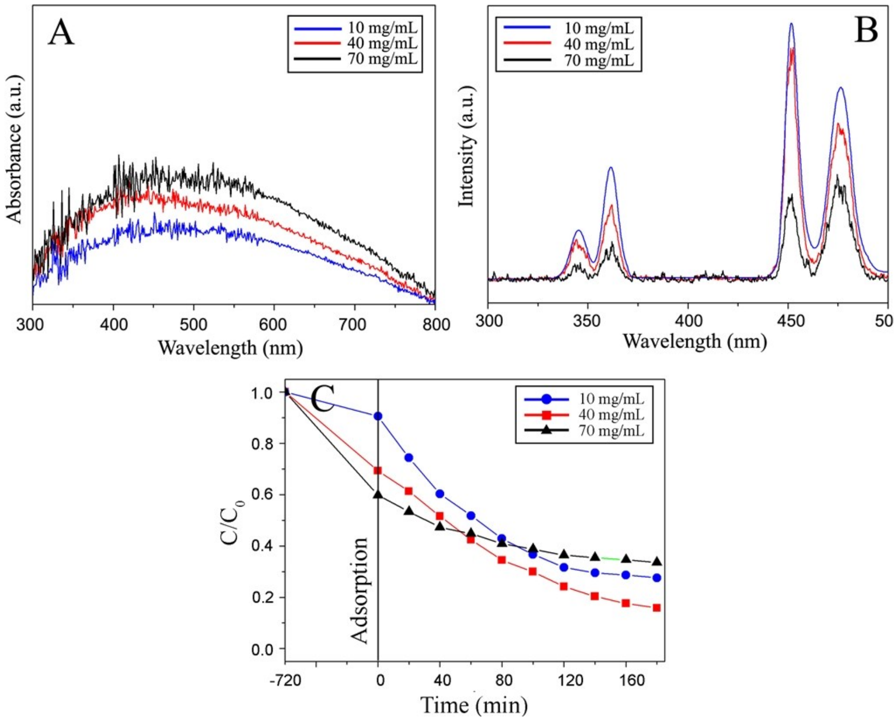

Figure S10. (A) UV-Vis spectra and (B) Upconversion spectra of $NaYF_4$:Yb,Tm@C NPs prepared with different concentration of glucose; (C) Comparison of photocatalytic activities of $NaYF_4$:Yb,Tm@C NPs with different carbon thickness after CdS deposition under the NIR band. The absorption of carbon shell increases along with the shell thickness and the UC emissions of $NaYF_4$:Yb,Tm@C NPs become decreased due to the absorption and scattering effect of the shell. After deposition of CdS NCs, thicker carbon shell enables better adsorption of dye molecules but increases the distance between $NaYF_4$:Yb,Tm and CdS. In contrast, thinner carbon shell sample exhibits short distance and strong UC emissions, but low adsorption to dye molecules. As such, a moderate carbon shell (i.e., 30 nm) is preferred for the consideration of both energy transfer and dye adsorption.